Aggregation-Free Gold Nanoparticles in Ordered Mesoporous Carbons: Toward Highly Active and Stable Heterogeneous Catalysts

Shuai Wang,[†] Qingfei Zhao,[†] Huimin Wei,[†] Jian-Qiang Wang,[‡] Minhyung Cho,[§] Hae Sung Cho,[§] Osamu Terasaki,[§] and Ying Wan*,[†]

[†]The Education Ministry Key Lab of Resource Chemistry, Shanghai Key Laboratory of Rare Earth Functional Materials, and Department of Chemistry, Shanghai Normal University, Shanghai 200234, P. R. China

[‡]Shanghai Synchrotron Radiation Facility (SSRF), Shanghai Institute of Applied Physics, Chinese Academy of Sciences, Shanghai 201204, P. R. China

[§]Graduate School of EEWS (WCU), Korea Advanced Institute of Science and Technology, Daejeon 305-701, Republic of Korea

S *Supporting Information*

ABSTRACT: A coordination-assisted synthetic approach is reported here for the synthesis of highly active and stable gold nanoparticle catalysts in ordered mesoporous carbon materials using triblock copolymer F127 as a structure-directing agent, thiol-containing silane as a coordination agent, $HAuCl_4$ as a gold source, and phenolic resin as a carbon source. Upon carbonization, the gold precursor becomes reduced to form monodispersed Au nanoparticles of ca. 9.0 nm, which are entrapped or confined by the "rigid" mesoporous carbonaceous framework. Nanoparticle aggregation is inhibited even at a high temperature of 600 °C. After removal of the silica component, the materials possess the ordered mesostructure, high surface area ($\sim$1800 m^2/g), large pore volume ($\sim$1.19 cm^3/g), and uniform bimodal mesopore size (<2.0 and 4.0 nm). The monodispersed gold nanoparticles are highly exposed because of the interpenetrated bimodal pores in the carbon framework, which exhibit excellent catalytic performance. A completely selective conversion of benzyl alcohol in water to benzoic acid can be achieved at 90 °C and 1 MPa oxygen. Benzyl alcohol can also be quantitatively converted to benzoic acid at 60 °C even under an atmospheric pressure, showing great advantages in green chemistry. The catalysts are stable, poison resistant, and reusable with little activity loss due to metal leaching. The silane coupling agent played several functions in this approach: (1) coordinating with gold species by the thiol group to benefit formation of monodispersed Au nanoparticles; (2) reacting with phenolic resins by silanol groups to form relatively "rigid" composite framework; (3) pore-forming agent to generate secondary pores in carbon pore walls, which lead to higher surface area, larger pore volumes, and higher accessibility to to the gold nanoparticles. Complete removal of the silica component proves to have little effect on the catalytic performance of entrapped Au nanoparticles.
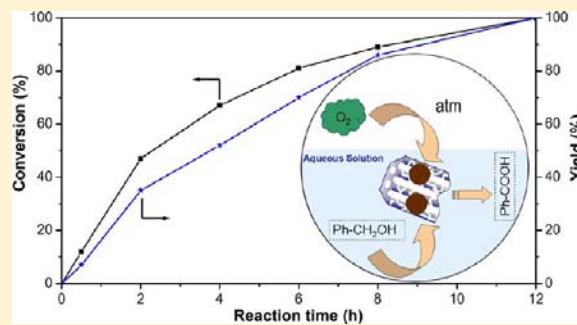
1. INTRODUCTION

Gold nanoparticles as catalysts are of great significance in oxidations, addition to multiple C−C bonds, cyclization reactions, rearrangements, and C−C coupling reactions.[1] Supporting carriers may disperse and fix the gold nanoparticles. The supports can range from oxides, for example, CeO_2,[2] and TiO_2,[3] mixed oxides including Mg−Al−O[4] and Ga−Al−O,[5] to polymers such as poly(N-vinyl-2-pyrrolidone) (PVP)[6] and poly(o-phenylenediamine) (PoPD).[7] However, particle growth at high temperatures, or even during reduction and reaction, accompanied by a corresponding loss of catalytic activity, is a serious problem. This is mainly caused by the increased mobility of the gold particles with low melting point on the carrier.[8] Additionally, the metal particles usually detach from the support in reuse, resulting in a sharp decrease in active sites.[9]

Recently, encapsulation of the dispersed gold nanoparticles inside porous silica, CeO_2, zeolite, etc. has been proved to enhance catalytic activity and impede nanoparticle sintering under high-temperature environments.[10] In particular, several groups individually reported the intercalation of monodispersed gold nanoparticles in the mesoporous silica and organosilica framework with the assistance of thiol-containing silane or silsesquioxane.[11] The presence of a protection shell or layer outside active metal cores has also been reported to be feasible for enhancing the thermal stability against sintering.[12] For example, Schueth and co-workers developed a bottom-up strategy for stable yolk-shell gold nanoparticles.[13] The gold nanoparticles are monodispersed in each zirconia-based sphere that inhibits the aggregation among particles at higher

temperatures. However, these oxide carriers undergo change during the heat treatment, as the surface area dramatically decreases. A facile route to stabilize monodispersed gold nanoparticles is still expected.

The advantages of carbon supports with respect to conventional oxidic supports, like silica and zirconia, involve the stable structure which can minimize the shrinkage effect on support up to 1000 °C under an inert atmosphere, chemical inertness, intrinsic hydrophobic nature, as well as easy recovery of precious metal active phases from spent catalysts by burning away carbon. The carbon-based palladium nanocatalyst has been proved to be a highly efficient catalyst in the water-mediated Heck coupling reaction.[14] By comparison, immobilization of monodispersed Au nanoparticles on activated carbon remains a challenge since the conventional methods such as deposition-precipitation (DP) and impregnation cannot be applied. For example, under normal conditions in the DP process, $AuCl_4^-$ cannot be effectively deposited onto a negatively charged acidic carbon surface due to electronic repulsion. The impregnation method is unfeasible, possibly due to the inert carbon matrix which shows weak interaction with gold nanoparticles and therefore cannot anchor tiny particles with high surface energy.[15]

Several attempts have been done to disperse stable gold nanoparticles on carbon by enhancing their interaction. Rossi and Prati first showed a colloidal synthesis for finely dispersed gold nanoparticles (AuNPs) on the activated carbon surface which involved the use of preformed gold colloids with protecting groups.[16] Hardacre and co-workers demonstrated that gold particles supported on activated carbon (Au/C) can be dispersed down to the atomic level during the carbonylation in the presence of methyl iodide.[15a] However, the treatment by methyl iodide may somewhat impede the catalytic activity in dehydrogenation. The random pore-size distribution of activated carbon ranging from micropores to macropores may also inhibit their applications where diffusion may be a rate-limiting step, for example, catalysis and adsorption. Vinu and co-workers directly used a nanocasting carbon nitride support with inbuilt functionalities that acts as a stabilizing, reducing, and pore-size-controlling agent to anchor gold nanoparticles via the traditional two-step method.[17] Tuel and co-workers also casted gold@mesoporous carbon coating using gold nanoparticles coated with a thiol-functionalized mesoporous silica shell as a sacrificed scaffold.[18] Gold@ordered mesoporous carbons with tailored pore sizes have been reported as a good candidate for given reactions in particular for the shape-selective ones. However, the stability, especially under high temperatures, is not reported. A repeated nanocasting was adopted to cast yolk-shell gold nanoparticles supported on carbon by using the above Au@ZrO$_2$ hard template.[15e] The porosity of the shell is imperfect, and the thick shell or micropores may influence diffusion of reactants. The catalytic activity may be inhibited. Up to now, no results have been reported related to the one-step synthesis of gold nanoparticles on mesoporous carbon matrix.

In this manuscript, we demonstrate a coordination-assisted self-assembly approach for the intercalation of aggregation-free and monodispersed gold nanoparticles inside the ordered mesoporous carbon frameworks, using triblock copolymer F127 as a structure-directing agent, HAuCl$_4$ as a gold source, preformed phenolic resins as a carbon source, and 3-mercaptopropyltrimethoxysilane (MPTMS) as a coordination and coupling agent. The strong coordination between the thiol group and Au species favors the immobilization of gold in the carbonaceous matrix. Upon carbonization and removal of silica, the carbon-supported catalysts possess the highly ordered mesostructure, high surface area of ~1800 m^2/g, large pore volume of ~1.19 cm^3/g, bimodal mesopores with uniform primary mesopore size of about 4.0 nm, and plenty of secondary mesopores less than 2.0 nm and monodispersed gold nanoparticles inside the matrix with a size of ~9 nm. Both the mesostructure and gold nanoparticles are sintering free at high temperatures up to 600 °C. The heterogeneous gold catalyst is highly active in selective aerobic oxidation of benzyl alcohol using water as a solvent, showing a conversion close to 100% at 90 °C under 1 MPa within 1 h and at 60 °C under an atmospheric pressure within 12 h. The mesoporous Au−C catalyst is stable and reusable. These advantages pave the way for supported gold nanoparticles in green chemistry.

2. EXPERIMENTAL SECTION

2.1. Chemicals. Poly(ethylene oxide)-*b*-poly(propylene oxide)-*b*-poly(ethylene oxide) triblock copolymer F127 (EO$_{106}$PO$_{70}$EO$_{106}$, M_w = 12 600) and 3-mercaptopropyltrimethoxysilane (MPTMS, minimum 98 wt %) were purchased from Acros Chemical Inc. Chloroauric acid tetrahydrate (HAuCl$_4$·4H$_2$O, Au minimum 47.8 wt %) and other chemicals were obtained from Shanghai Chemical Company. All chemicals were used as received without any further purification. Water used in all experiments was deionized.

2.2. Synthesis of Ordered Mesoporous Au−C Catalysts. The synthesis involves coordination-assisted self-assembly of low-polymerized phenolic resins, MPTMS, tetraethylorthosilicate (TEOS), HAuCl$_4$, and triblock copolymer F127 template. In a typical synthesis, 2.08 g of TEOS and 1.97 g of MPTMS were first mixed in the presence of 10.0 g of ethanol for 30 min. At the same time, 3.2 g of Pluronic F127, 2.0 g of HCl (0.2 M), and 10.0 g of ethanol were mixed together to obtain a clear solution. To it, 6.3 mL of HAuCl$_4$ solution (gold concentration in ethanol: 48.5 mmol/L) was added. After stirring for 10 min, the mixtures of TEOS and MPTMS and a solution containing 2.0 g of preformed phenolic resins and 8.0 g of ethanol were added in sequence. The low-polymerized phenolic resins were prepared according to the established procedure as described in Supporting Information (SI). After stirring for 2 h at 40 °C, the mixture was poured into multiple dishes. The dishes were placed in a hood to evaporate ethanol at 40 °C for 5 h and then to thermopolymerize at 100 °C for 24 h. The as-made films were scratched from the dishes and ground into fine powders. Calcination was carried out in a tubular furnace under nitrogen flow to obtain mesoporous gold−polymer−silica or gold−carbon−silica nanocomposites. The temperature program was from room temperature to 350 °C with a ramp of 1 °C/min, to 600 with 5 °C/min, and maintenance for 3 h. The catalyst was denoted as Au(SH)−SC. Then, the gold−carbon−silica nanocomposite was immersed with NaOH aqueous solution (1 M) at 45 °C four times to remove the silica component. Each time took 12 h. The sample was named as Au(SH)−C. The catalysts were dried in an oven at 80 °C overnight under vacuum and then at 150 °C for 4 h in air.

For comparison, thiol-group-free Au(0)−SC and gold-free (SH)−SC samples were synthesized according to the above procedure with the maintenance of the total silica and/or gold contents.

2.3. Characterization. The powder X-ray diffraction (XRD) measurements were taken on a Rigaku Dmax-3C diffractometer using Cu Kα radiation (40 kV, 20 mA, λ = 0.15408 nm). The metallic Au sizes were estimated according to the Scherrer formula: size = $0.89\lambda/\beta \cos\theta$ on the basis of the 111 diffraction peak in wide-angle XRD patterns. N$_2$ adsorption−desorption isotherms were measured at 77 K with a Micromeritics TriStar II 3020 analyzer. The Brunauer−Emmett−Teller (BET) method was utilized to calculate the specific surface areas (S_{BET}). By using the Barrett−Joyner−Halenda (BJH) model, the pore volumes and pore size distributions were derived from the adsorption branches of isotherms. Transmission electron

microscopy (TEM) experiments were conducted on a JEM 2100 microscope operated at 200 kV. Energy-dispersive X-ray spectroscopy (EDX) was performed on a Philips EDAX instrument. Scanning electron microscopy (SEM) images of Au(SH)−C were taken with a JSM-7600F operated at 15 kV. SEM specimens were prepared by fixating powder to the SEM sample holder using carbon paste. To observe pore network structure inside the sample, IB-09010CP was used for cross-section polishing at 4 kV during 14 h. The sample was put on a silicon wafer by carbon paste and then placed in a cross-section polisher. Fourier transform infrared (FT-IR) spectra were collected on a Nicolet Fourier spectrophotometer. Thermal gravimetric analysis (TG) curves were monitored on a Mettler Toledo 851e apparatus. X-ray photoelectron spectroscopy (XPS) measurements were performed on a Perkin-Elmer PHI 5000CESCA system with a base pressure of 10^{-9} Torr. Au contents are determined by inductively coupled plasma−atomic emission spectrometry (ICP−AES, Varian VISTA-MPX). X-ray absorption spectra at the Au L_3 edge of samples were collected in the fluorescence mode on the BL14W1 of the Shanghai Synchrotron Radiation Facility (SSRF). The data processing was performed using the program ATHENA. All fits to the EXAFS data were performed using the program ARTEMIS. UV−visible diffuse reflectance spectra were recorded on a Varian Cary 300 Scan UV−visible spectrophotometer, with an integrating sphere attachment using $BaSO_4$ as the background standard. The real-time UV−vis spectra were determined using a Varian Cary 100 ultraviolet−visible spectrophotometer.

2.4. Activity Test. The high-pressure oxidation reactions were carried out in a 50 mL autoclave reactor. The vessel was charged with catalyst (10 mg), benzyl alcohol (4.8 mmol), H_2O (10 mL), and KOH (14.4 mmol). The autoclave was then purged five times with oxygen, leaving the vessel at the 1 MPa gauge. Then the reaction mixture was raised to 90 °C. In an atmospheric reaction, the same reagents were placed in a 25 mL flask. Molecular oxygen was then introduced into the flask from an O_2 balloon under atmospheric pressure, and the mixture was heated to 60 °C with stirring.[19] At different time intervals, hot filtration was adopted to determine the Au leaching and benzyl alcohol conversion. The catalyst was separated and submitted to continuous solid−liquid extraction with ethyl acetate (5 mL) using a micro-Soxhlet equipment. Then the solid catalyst was washed by a copious amount of water and dried at 80 °C overnight under vacuum for reuse. The extracted solution was mixed with the reaction solution which was first neutralized with HCl solution and extracted with ethyl acetate (15 mL). The mixtures were weighed and analyzed. The recovered material accounted for more than 95% of the starting material. The benzyl alcohol oxidation was repeated three times, yielding the same initial rates and total reaction times within ±10%. For the identification and analysis of the products, GC−MS equipped with a capillary DB-Wax column was used by comparison with authentic samples. The analysis was repeated at least three times for all tests, and the experimental errors were within ±5%. Catalytic results were shown in terms of absolute yield of benzoic acid; conversion of benzyl alcohol; initial rate (*mmol of reacted benzyl alcohol per g of catalyst and hour*) calculated at the beginning of the reaction and turnover number (TON, *initial rate/total Au concentration*).[20]

For the thiourea poisoning experiment, a solution of thiourea, which was prepared by dissolving the proper amount in Milli-Q water, was added as a solvent. In standard experiments under an atmospheric pressure, the reaction was performed for 6 h to ensure incomplete conversion of benzyl alcohol allowing for a comparison of the activity of the poisoning catalyst.[20,21]

For recycling study, selective oxidation was performed with benzyl alcohol and oxygen maintaining the same reaction conditions as described above except using the recovered catalyst. Several parallel reactions were carried out to ensure that the catalyst amount was the same in each run. The reused catalyst was designated as Au(SH)−C−Ry, wherein y was catalytic run. For example, Au(SH)−C−R2 represented the catalyst that was used in the second run.

3. RESULTS

3.1. Location and Thermal Stability of Gold Nanoparticles. Figure 1 shows the small-angle (SAXRD) and wide-
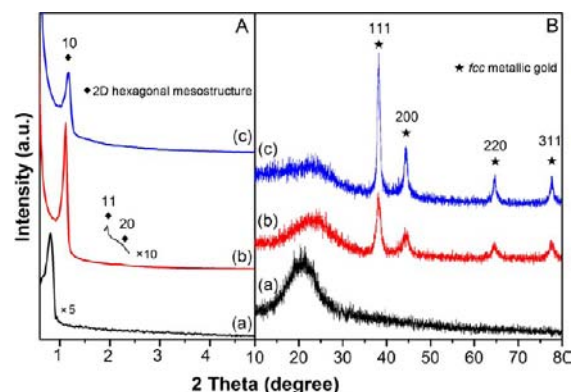

Figure 1. SAXRD (A) and WAXRD (B) patterns for gold-containing mesoporous catalysts (a) as-made Au(SH)−SC, (b) Au(SH)−SC, and (c) Au(SH)−C.

angle XRD (WAXRD) patterns for Au-containing mesoporous carbon-silica catalysts. The distinct diffraction peaks can be detected in the SAXRD pattern for the as-made Au(SH)−SC, indicative of an ordered mesostructure with *p6mm* space group.[22] Only one strong diffused diffraction peak at 2θ about 22° is displayed in the WAXRD pattern, implying the amorphous framework. The FT-IR spectrum of as-made Au(SH)−SC clearly shows bands at ∼3400, 3000−2800, 1610, 1460, 1100, and 960 cm^{-1} (SI Figure S1). The bands at ∼3400 cm^{-1} can be assigned to the −OH stretching, coming from both organic and inorganic components, i.e., a large amount of phenolic −OH groups, uncross-linked benzyl alcohol, and silanol groups.[22,23] The presence of the organic Bakelite component can be proved by the bands at ∼3000−2800, 1610, and 1460 cm^{-1}, which can be attributed to the C−H and C−C bond stretching of trisubstituted and phenyl-alkyl ether-type-substituted aromatic ring structures or other characteristic stretching modes of phenolic resins. The bands at ∼1100 and 960 cm^{-1} can be assigned to the characteristic Si−O−Si and Si−OH vibrations. Several bands at ∼1100 and 3000−2800 cm^{-1} can be attributed to the C−O and C−H stretching of copolymer F127. However, the thiol group in IR is invisible under the current conditions, perhaps due to the weak dipoles exhibited by S−H groups which make their modes difficult to be detected by vibrational spectroscopy.[24]

Carbonization of the materials is carried out at 600 °C. The vibrations in the FT-IR spectrum for Au(SH)−SC belonging to the polymer disappear, implying the conversion from polymeric to carbonaceous framework and the reserve of vibrations belonging to Si−O bonds, confirming the presence of the silica component (SI Figure S1). The EDX spectrum confirms the elements of Au, C, Si, and O in the catalyst (Figure 3A, inset). The undetectable sulfur element proves the release of the −SH group during calcination. The gold content, determined by the ICP−AES analysis, is about 2.6 wt %.

Besides the diffused peaks at 22°, the peaks at 2θ of 38, 44, 65, and 78° are also observed in the WAXRD pattern for Au(SH)−SC, attributed to the 111, 200, 220, and 311 diffractions of face-centered cubic (fcc) metallic gold (JCPDS PDF-04-0784). The {111} lattice space is estimated to be 0.24 nm. The diffractions are wide, implying tiny nanoparticles.

Table 1. Structural and Textural Parameters for Gold-Containing Mesoporous Catalysts

sample	Au content[a] (wt %)	a_0[b] (nm)	S_{BET} (m²/g)	V_t (cm³/g)	D_p (nm)	d_{Au}[c] (nm)	d_{Au}[d] (nm)
As made Au(SH)−SC	n.d.	12.7	---	---	---	---	---
Au(SH)−SC	2.6	9.1	418	0.29	4.2	9.2	8.7
Au(SH)−C	5.9	8.9	1826	1.19	4.0	9.4	8.9
Au(0)−CS	n.d.	11.6	413	0.50	6.9	50	n.d.
Au(0)−C	n.d.	11.0	1331	1.23	6.0	50	150
(SH)−C	---	8.6	1621	1.06	4.1	---	---
Au(SH)−C−R2	5.9	8.6	1693	1.11	3.9	9.5	9.5
Au(SH)−C−R4	5.9	8.5	1624	1.06	3.8	9.6	n.d.

[a]Estimated by ICP−AES and TG analysis. [b]Cell parameter of the mess structure. [c]Calculated from the Scherrer formula according to the 111 diffraction. [d]Estimated from TEM analysis of average diameter.

Estimation with the Scherrer formula gives rise to the gold particle size of about 9.2 nm (the size of perpendicular to the 111 plane, the same in the latter). If 200, 220, and 311 diffractions are applied for estimation, the particle size even reduces to about 7 nm. No diffraction belonging to gold oxides is found. The well-resolved SAXRD pattern for Au(SH)−SC can be retained, with a slight shift to higher 2θ values compared to that for the as-made sample, suggesting the stable mesostructure framework with a small shrinkage (about 28%). The unit-cell parameter (a_0) of the mesoporous structure with $p6mm$ is calculated to be 9.1 nm (Table 1). N_2 sorption isotherms of Figure 2 display typical type-IV curves with
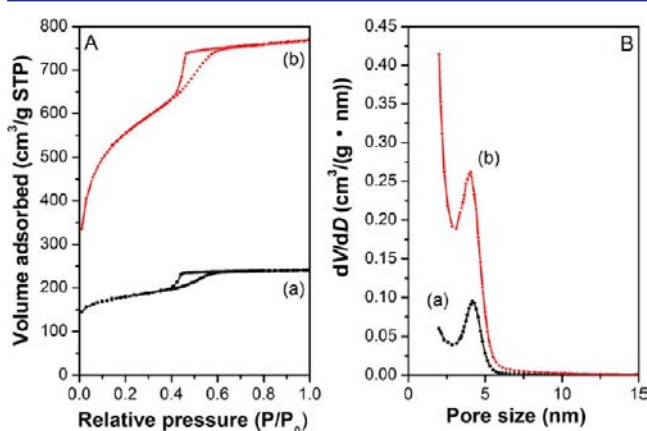

Figure 2. N_2 sorption isotherms (A) and pore size distribution curves (B) for mesoporous carbonaceous catalysts containing aggregation-free and well-dispersed gold nanoparticles before and after removal of silica: (a) Au(SH)−SC and (b) Au(SH)−C.

distinct capillary condensation steps for Au(SH)−SC, characteristic of mesoporous solids with uniform pore size. This phenomenon is coincident with the XRD pattern. A narrow pore-size distribution curve with the mean value of 4.2 nm is calculated from the adsorption branch. The hysteresis loop for the catalysts belongs to the H2 type. Desorption occurs at relative pressures close to the fluid cavitation pressure.[25] This phenomenon has also been observed in mesoporous carbon FDU-15 and carbon−silica composites with the highly ordered 2D hexagonal mesostructure, which may be originated from the nonuniform pore surface of carbon materials, as well as partially blocked larger mesopores.[22,23b,26] The BET surface area is 418 m²/g, and the pore volume is 0.29 cm³/g for the Au-containing mesoporous silica−carbon catalyst. The estimated pore wall thickness is 4.9 nm, on the basis of the hexagonal pore structure. It should be noted that the gold nanoparticle size is

apparently larger than either the pore size or wall thickness. The result implies that gold particles occupy both pore space and wall.

TEM images for Au(SH)−SC further confirmed the stable ordered 2D hexagonal mesostructure ($p6mm$) with hexagonally arranged pores (Figure 3). Notably, monodispersed gold nanoparticles which locate inside mesochannels with expansion to the pore walls are found within the whole catalyst particles. Distortion in ordered porosity caused by deposition of Au nanoparticles is unobvious. The ordinate in Figure 3C presents a normalized number (0−150) of particles, revealing nanoparticles with a mean size of 8.7 nm. No large particles aggregates were observed in TEM images, which suggests that the monodispersed gold nanoparticles are incorporated in the mesopores of carbonaceous matrix. This is directly confirmed by the following SEM observations.

The XPS analysis is a surface-sensitive technique with a sampling volume that extends from the surface to a depth of 1−5 nm.[27] The diffused peaks with binding energy of about 84 and 88 eV can be assigned to $Au_{4f5/2}$ and $Au_{4f7/2}$ in the metallic state (Figure 4). However, these two XPS signals are extremely weak. The surface and near-surface concentration of metallic gold is far lower than the value from the ICP−AES analysis. This observation can be attributed to the immobilization of gold particles in the pore system, confirming the previous conclusion from electron microscopy analysis. Similar phenomena have been reported by Lu et al. and our group.[28] The binding energy signals for nickel or iron are extremely weak for metal-containing mesoporous carbons in which metal or oxide nanoparticles are involved inside the mesopore walls. Only Au, C, O, and Si are detected, confirming the absence of any contamination from chlorine and sulfur for the catalyst.

3.2. Gold Nanoparticles in Mesoporous Carbon with a High Surface Area. A further step to dissolve the silica component from the integrated silica−carbon frameworks was carried out. The Si signals disappear, and the O signals pronouncedly reduce in the XPS spectrum for the Au(SH)−C catalyst (Figure 4), proving the elimination of SiO_2. The EDX pattern further reveals the absence of element Si (Figure 3D inset). The ICP−AES analysis displays that Au(SH)−C has a gold content of 5.9 wt %. Gold ions are undetectable in the collected basic solution after immersing with the gold-containing catalyst, suggesting the stability of gold nanoparticles and negligible leaching during etching of silica.

The mesoporous pure carbon-based gold catalyst Au(SH)−C shows well-resolved SAXRD and WAXRD patterns (Figure 1), proving the maintenance of the 2D hexagonal mesostructure, and fcc Au nanoparticles with a size about 9.4 nm. TEM images confirm the above results (Figure 3D−F). Both
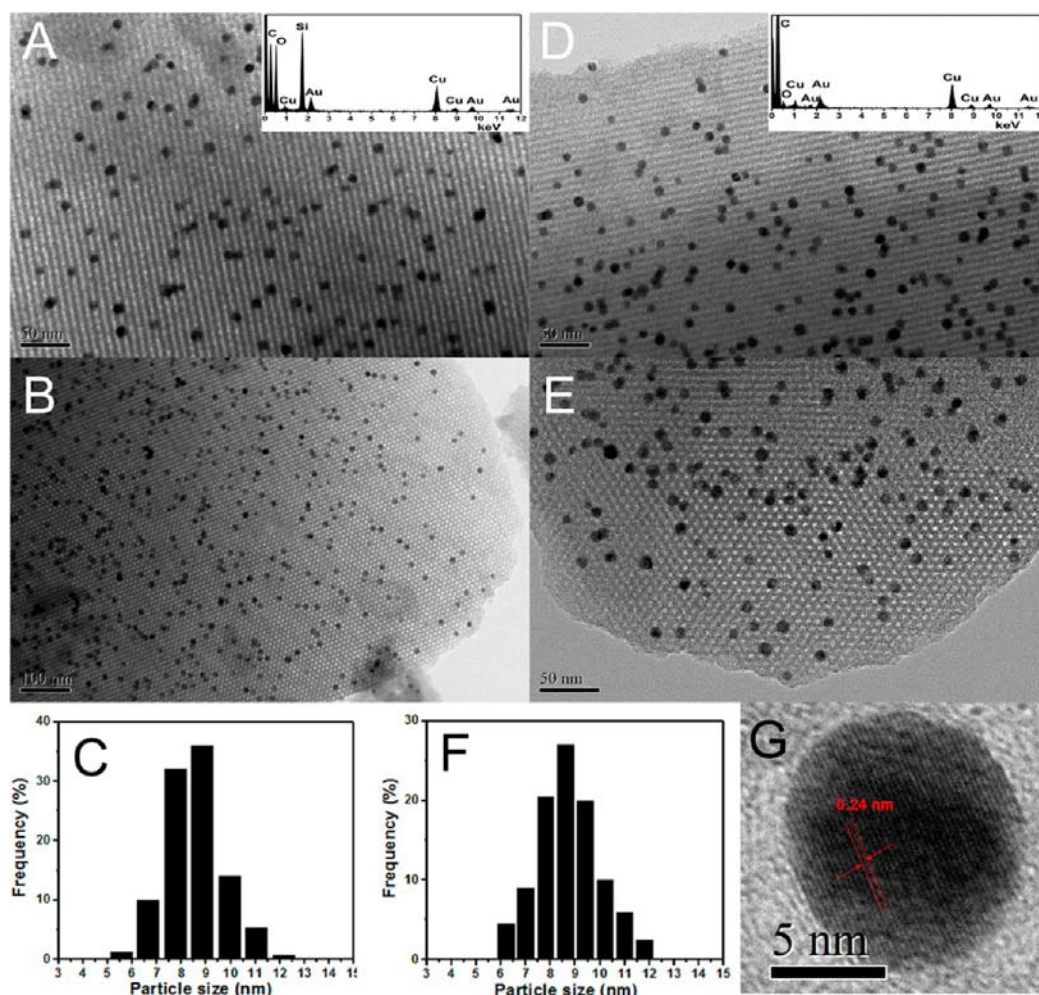
Figure 3. TEM images (A, B, D, E) and metal particle size distribution histogram (C, F) for the self-assembled Au(SH)−SC catalyst (A−C) and this catalyst after etching of the silica component Au(SH)−C (D−F), viewed along the [11] (A, D) and the channel directions (B, E). Insets (A) and (D) are EDX patterns. (G) HRTEM of a representative gold nanoparticle in (D).
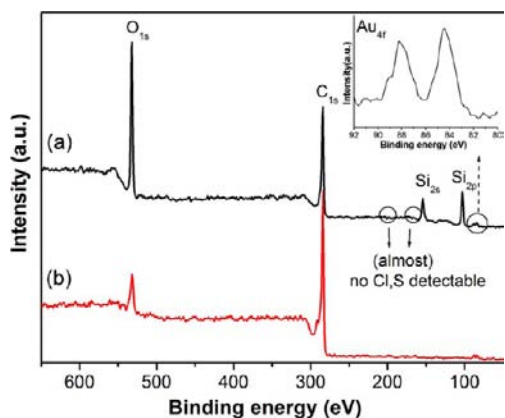

Figure 4. XPS spectra of mesoporous catalysts with well-dispersed gold nanoparticles confined inside frameworks: (a) Au(SH)−SC and (b) Au(SH)−C. Inset is magnification of XPS spectra for Au$_{4f}$.

the ordered pore arrays and the sintering-free and well-dispersed nanoparticles with a mean size of about 9.0 nm are presented. Figure 3G shows a representative particle, revealing the characteristic lattice fringes of 0.24 nm of Au{111}. By comparison with the images for the mother Au(SH)−SC catalyst, we can observe neither a distinct migration nor growth

of gold nanoparticles. The particles, which locate inside mesochannels with expansion to the pore walls, stay intact, although the pore walls of the carbon mesostructure seem looser than the mother catalyst. These observations further suggest that the removal of the silica component has a minor effect on both the mesostructure and gold nanoparticles.

SEM can give an elemental distribution map through images of back-scattered electrons (BSEs) and EDS as well as surface topographic information through those of secondary electrons (SEs). In order to find positions of Au nanoparticles either external surfaces or internal mesopores, SEM images for both the surface and cross-section of Au(SH)−C were observed through images of mixed BSEs and SEs (Figure 5). A typical rough surface of mesoporous carbon solids with opened mesopores is observed. Large gold nanoparticles are hardly observed on the external surface. After cross-sectioning, Au nanoparticles within the mesoporous carbon pore network appear as bright Z-contrast (which are confirmed to be Au by EDS). The brighter contrast of the Au nanoparticle at the top left of Figure 5B corresponds to the particle exposed to the surface, while the other two particles are covered with thin carbons, confirming the entrapping of gold nanoparticles in carbon internal mesopores. Sizes of carbon pores and Au nanoparticles are measured, as shown in the image (gold
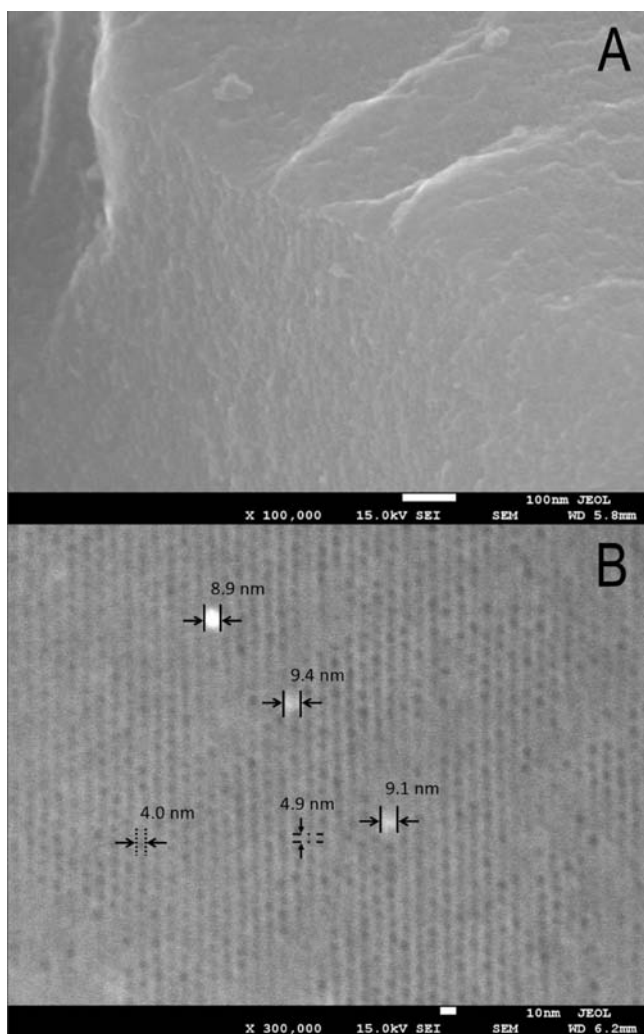
Figure 5. HRSEM images for the Au(SH)−C surface (A) and after cross-section polishing (B). All images were taken at 15 kV with 5.8 mm (A) and 6.2 mm (B) of working distances. The particle sizes are labeled with a solid line, the primary mesopore size is labeled with a dotted line, and the wall thickness is labeled with a dash-dotted line.

particle size, primary pore, and wall thickness of ∼9.1, 4.0, and 4.9 nm, respectively), which are analogous to the values calculated from the N_2 sorption and WAXRD results. Though the size of Au nanoparticles is obviously larger than that of pores, the carbon network was not severely damaged by gold deposition.

Besides a capillary condensation at middle relative pressures in the N_2 isotherm curves, a remarkable sorption at relative pressure of P/P_0 of 0.01−0.3 is observed for Au(SH)−C (Figure 2), compared with its mother composite Au(SH)−SC. Accordingly, Au(SH)−C possesses an extremely high BET surface area of 1826 m^2/g and large pore volume of 1.19 cm^3/g, which is almost 4 times higher than the mother catalyst, and a bimodal-like pore-size distribution with the most probable pore sizes of 4.0 and less than 2.0 nm. The primary mesopore size is similar to Au(SH)−SC, while the secondary one is much smaller. Since the micropore volume of Au(SH)−C is low (SI Figure S2), the secondary mesopores contribute the majority of surface area and pore volume. These phenomena have also been observed for mesoporous silica−carbon materials.[14,22] Silica and carbon can form an interpenetrating framework.

Once silica nanoparticles are etched, plenty of voids (<2 nm secondary mesoproes) are formed inside carbon pore walls. Therefore, the original mesoporous Au(SH)−SC composites also possibly possess an interpenetrating inorganic−inorganic framework instead of a carbon coating on mesoporous silica. Upon removal of the silica component, secondary voids are generated inside the carbon walls. Gold nanoparticles are free of immigration and aggregation because of the confinement by carbon walls and mild washing by NaOH solution. The penetrated voids in walls can therefore provide high surface area and, more importantly, high accessibility to gold nanoparticles which partially locate inside pore walls. In addition, the generation of edges in the interface between carbon and gold can therefore be expected.

3.3. Role of the Thiol Group. A reference sample Au(0)−SC was synthesized with the same procedure as Au(SH)−SC but in the absence of MPTMS. Au(0)−SC shows a well-resolved SAXRD pattern (SI Figure S3A), indicating the highly ordered mesostructure with the domain size calculated to be 11.6 nm. The pore size distribution for this catalyst is also narrow, centered at about 6.9 nm (SI Figure S4). However, the WAXRD pattern of Au(0)−SC gives very sharp diffractions for fcc Au (SI Figure S3B), implying the presence of large Au particles with a diameter above 100 nm. The phenomenon implies the macrophase separation of the ordered mesostructure and large metallic particles.[28b] TEM images indeed show both ordered mesostructure domains without distinct nanoparticles and large particle aggregation outside the carbonaceous support even heating at 600 °C (SI Figure S5). EDX analysis reveals that no gold nanoparticles can be detected in the ordered domains (SI Figure S5B inset).

We thereafter traced the synthesis in the absence/presence of MPTMS with the real-time UV−vis spectra (Figure 6A). The pristine ethanolic $HAuCl_4$ solution with yellowish color exhibits an absorption band centered at 320 nm, which is attributed to the ligand metal $\pi \rightarrow \sigma^*$ orbital transition in $(AuCl_4)^-$ species. Negligible changes in the solution color and UV−vis spectra can be found after successive addition of triblock copolymer F127 and TEOS. Pronounced difference takes place once the pristine solution contains functional monomer MPTMS. The solution varies to colorless. The absorption intensity due to the $\pi \rightarrow \sigma^*$ orbital transition decreases dramatically, suggesting the disappearance of Au−Cl coordination.[29] A further addition of low-polymerized phenolic resin can only generate several strong absorptions below 300 nm, which are originated from the benzene-ring frameworks, but shows a minor effect on the absorption by Au species. Individual interactions between ethanolic $HAuCl_4$ solution with reactants were also investigated (SI Figure S6). The remarkable change in absorbance by Au species occurs only with the presence of MPTMS, that is, a distinct reduction in intensity of the band at 320 nm assigned to the Au−Cl coordination. These observations demonstrate the change in the coordination atoms with Au from Cl to S.[30]

Figure 7 shows the XANES data at the Au L_3 edge for the synthetic solutions of Au(SH)−SC and thiol-free Au(0)−SC, a Au^{3+} reference of $HAuCl_4$ solution and gold foil. The thiol-free synthetic solution for Au(0)−SC displays a spectrum of shapes and edge energies similar to the Au^{3+} reference, which exhibits a large absorption feature at a lower binding energy (labeled a) than the bulk gold metal. This shift to a lower binding energy is due to the 2p to 5d transition that precedes the excitation to the bulk.[31] The results indicate that gold in thiol-free synthesis solutions is in the Au^{3+} state and the coordination with Cl, the
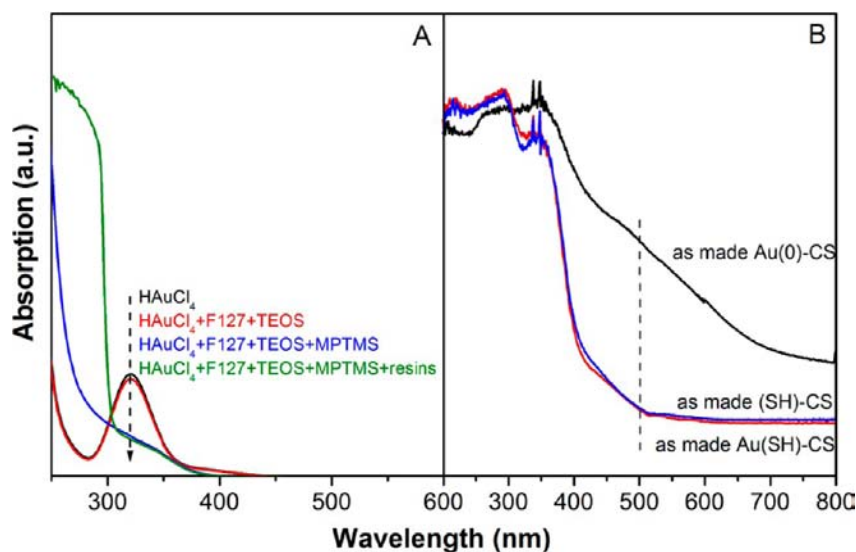
Figure 6. Real-time UV−vis spectra (A) of the synthetic solution of pristine ethanolic HAuCl$_4$ solution and the successive addition of triblock copolymer F127 and TEOS (red line), MPTMS (blue line), and phenolic resins (green line) and UV−vis spectra (B) of as-made Au(SH)−SC, Au(0)−SC, and (SH)−SC.
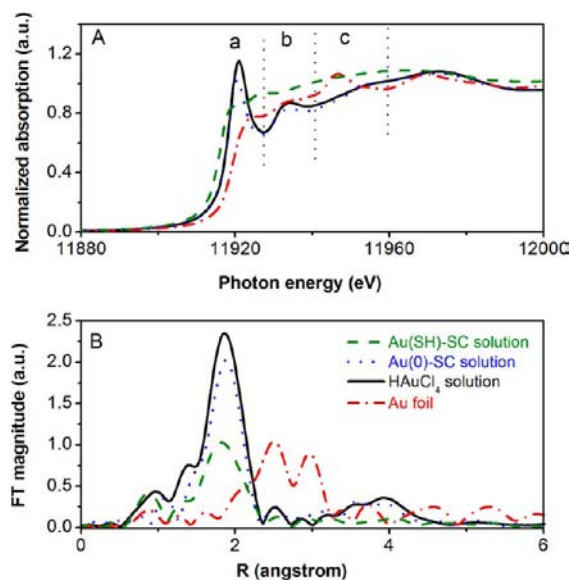

Figure 7. Au L$_3$ edge XANES (A) and Fourier transform of Au L$_3$ edge EXAFS (B) spectra of the synthesis solutions for Au(SH)−SC and thiol-free Au(0)−SC catalysts and the reference aqueous HAuCl$_4$ solution and Au foil.

same as the pristine HAuCl$_4$ solution. The spectrum for Au(SH)−SC synthesis solution has a left-shift binding energy, a much smaller a-feature, and weakened b- and c-features, probably due to a small concentration of 5d holes, implying

the distinct reduction in valence and change in the coordination state.[32] The reduction of Au(III) species to Au(I) thiolate has also been demonstrated by the thiol-containing PTMP−PMAA ligand,[33] p-HSCH$_2$(C$_6$H$_4$)C(CH$_3$)$_3$,[34] etc.

The Fourier transforms of the EXAFS data for the thiol-free synthesis solution of Au(0)−SC is very similar to the HAuCl$_4$ solution reference. Both show a strong Au−Cl coordination on the first shell with the bond length of about 2.29 Å and a coordination number (CN) of about 3 (Figure 7B, Table 2), indicating the maintenance of the gold state and coordination in the pristine solution. By comparison, the synthesis solution of Au(SH)−SC displays a strong coordination between Au and S, with a CN of 2 and a bond length of 2.30 Å. The replacement of the Au−Cl by Au−S bond is in coincidence with the UV−vis spectra. Neither Au(SH)−SC nor thiol-free Au(0)−SC solution exhibits a similar shape, edge energy, and Au−Au coordination to Au foil, excluding the reduction of metallic gold nanoparticles in solution.[35]

The as-made thiol-free Au(0)−SC displays a wide absorption band centered at about 500 nm due to the metallic Au surface plasma resonance, indicating the reduction of gold ions to metal at 100 °C. The WAXRD pattern for the as-made Au(0)−SC indeed shows the diffraction peaks belonging to metallic gold nanoparticles (SI Figure S7). On contrast, a featureless UV−vis spectrum is observed for the as-made Au(SH)−SC material, indicating the absence of gold nanoparticles and the reserve of the Au−thiol complex (Figure 6B). It should be noted, however, that gold clusters having less than 2 nm in diameter do not exhibit a generally intense surface plasmon

Table 2. Fit Parameters of Au L$_3$ Edge EXAFS Spectra for the Synthetic Solutions of Au(SH)−SC and Thiol-Free Au(0)−SC Catalysts and the Reference Aqueous HAuCl$_4$ Solution and Au Foil

sample	shell	N^a	R^b	σ^2 (10^{-3} Å^2)^c	ΔE_0 (eV)^d
solution for Au(SH)−SC	Au−S	2.0 ± 0.2	2.30 ± 0.01	2.2 ± 0.9	7.5 ± 1.1
solution for Au(0)−SC	Au−Cl	3.0 ± 0.6	2.29 ± 0.01	2.5 ± 1.6	11.2 ± 2.8
HAuCl$_4$ solution	Au−Cl	3.5 ± 0.4	2.27 ± 0.01	1.9 ± 1.0	9.1 ± 0.9
Au foil	Au−Au	10.6 ± 0.8	2.86 ± 0.01	8.3 ± 0.5	5.2 ± 0.5

^{a}Coordination number. ^{b}Distance between absorber and backscatterer atoms. ^{c}Debye−Waller factor. ^{d}Inner potential correction.

band.[36] Thus, the gold clusters, if formed, are very small. No characteristic UV−vis absorption can be observed for all carbon-based catalysts after carbonization due to strong absorption of light by carbon.

A gold-free sample (SH)−C was also synthesized. The reaction occurring between preformed phenolic resols which have plenty of phenyl or benzyl hydroxyl groups and a silane coupling agent containing reactive thiol groups facilitates the coassembly of mesostructure. The phenolic resin-based composites have the ordered mesostructure and high-content, chemically accessible thiol groups which can adsorb heavy metal ions and be further oxidized to sulfonic acid.[23b,37] After carbonization, the rigid silica−carbon framework was obtained.[37] A further etching step in basic solution leads to the formation of carbon solid with an ordered mesostructure, a cell parameter of 8.6 nm, a pore size of 4.1 nm, and a high surface area of 1621 m²/g (SI Figures S8 and S9, Table 1). These features are analogous to those for the Au(SH)−C catalyst. The results confirm the formation of rigid framework in the gold-containing mesoporous catalyst from the coassembly of MPTMS, TEOS, and phenolic resin, as well as the minor effect on mesostructure by gold deposition.

3.4. Selective Aerobic Oxidation of Benzyl Alcohol in Water.

Organic reactions in water have been extensively investigated for the fine and pharmaceutical chemical industries, due to the fact that they offer the possibility of providing environmentally benign reaction conditions by reducing the burden of the organic solvent disposal.[38] The oxidation of alcohols to carbonyl compounds in water under mild conditions is highly desired.

The selective oxidation of benzyl alcohol with molecular O_2 in water was chosen as a probe reaction to evaluate the activities of gold nanoparticles inside ordered mesoporous carbon frameworks. Using potassium hydroxide as a base, the reaction over Au(SH)−C is rather fast under 90 °C and 1 MPa (Figure 8). An almost complete conversion of benzyl alcohol to benzoic acid is achieved within 60 min. To the best of our knowledge, this is one of the highest activities for a selective oxidation of benzyl alcohol over a heterogeneous catalyst in water (SI Table S1).[6,7,39] A mild condition of 60 °C and atmospheric pressure was then adopted. The initial reaction rate reduces to 115.2 mmol g⁻¹ h⁻¹ with a TON value of 384
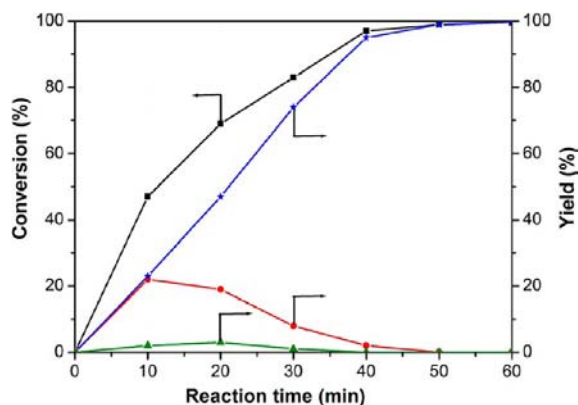
h⁻¹. However, benzyl alcohol can still almost complete selectively oxidized to benzoic acid within 12 h (Figure 9). The atomic economic reaction with a 100% yield in the presence of green solvent of water under atmospheric pressure shows great advantages in green chemistry.
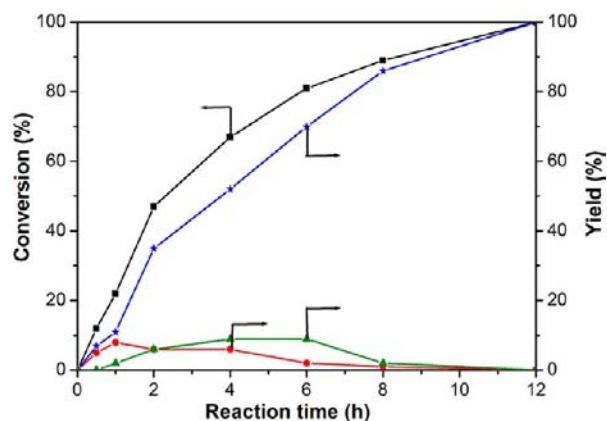

Figure 9. Time course plots for the conversion of benzyl alcohol (-■-) and yields of benzoic acid (-★-), benzaldehyde (-●-), and benzyl benzoate (-▲-) over fresh Au(SH)−C under atmospheric pressure (10 mg of catalyst (0.003 mmol of Au), 4.8 mmol of benzyl alcohol, 10 mL of water, 14.4 mmol of KOH, and 60 °C).

It should be noted that both benzaldehyde and benzyl benzoate are formed together with benzoic acid during reaction regardless of pressure and temperature. The yields for byproducts are low, with a maximum of 22% for benzaldehyde at 10 min and 3% for benzyl benzoate at 20 min under 1 MPa. With the prolongation of reaction, the selectivity for these substances reduces. At a reaction time of 50 min under high pressure or 12 h under atmospheric pressure, benzoic acid is detected as the exclusive product. This observation may suggest the intermediate of benzaldehyde during the oxidation from benzyl alcohol to benzoic acid. Esterification is possibly responsible for the formation of benzyl benzoate that was also found by Tsukuda and co-workers using the PVP-stabilized gold nanoclusters as a catalyst.[6] Accompanied with the conversion of most reactant, benzyl benzoate hydrolyzes and disappears.

Figure 10 shows the normalized conversions of the reaction as a function of the concentrations of thiocyanate. Note that the concentrations of thiocyanate are shown relative to the total
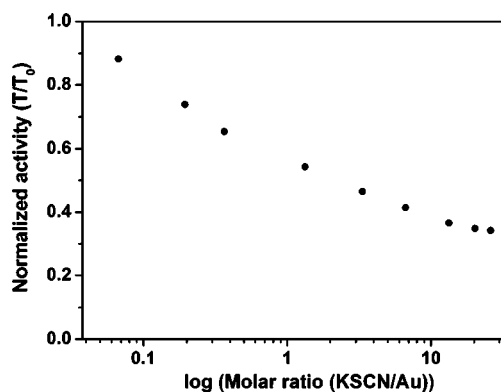

Figure 8. Time course plots for the conversion of benzyl alcohol (-■-) and yields of benzoic acid (-★-), benzaldehyde (-●-), and benzyl benzoate (-▲-) over Au(SH)−C with the reaction conditions: 10 mg of catalyst (0.003 mmol Au), 4.8 mmol of benzyl alcohol, 10 mL of water, 14.4 mmol of KOH, 1 MPa O_2, and 90 °C.

Figure 10. Residual activity after addition of various amounts of potassium thiocyanate for Au entrapped in mesoporous carbon.

number of Au atoms. The gradual addition of the poison to the catalyst gives rise to a slow decay of the catalytic activity. The conversion reduces only by 50% on adding an equal molar amount of NCS^- and Au_{total}. Even with a molar ratio of NCS^-/Au = 33, about 37% activity can be retained. It is much different from the heterogeneous Au catalysts showing a dramatic decrease in activity with addition of S-containing compounds.[20] For example, addition of 6 mol % of thiourea/Au_{total} leads to an almost complete loss of selective oxidation activity for glucose over Au/C.[20] Baiker and co-workers had found that the competitive adsorption of substrate over poison could improve the poisoning resistance.[21a] We would also like to contribute the interesting poison-resistance behavior over mesoporous Au-containing carbon catalyst to the strong adsorption of benzyl alcohol. The majority of thiocyanate is residue in water solution that may be inaccessible to gold nanoparticles. The high activity can therefore be retained at a high poison concentration. This result may further confirm the intercalation of gold nano-particles inside a carbon matrix instead of anchoring on the external surface of a particle. The poisoning mechanism deserves to be separately reported.

One of the key factors that must be considered for heterogeneous catalysts operating in three-phase systems is the possibility that active components can leach into the reaction mixture, leading to catalyst deactivation or formation of an active homogeneous catalyst. The liquid phase of the reaction mixture is collected by hot filtration after reactions. This operation can avoid the redeposition of any soluble species on the support during cold centrifugation. ICP−AES analysis confirms an undetectable amount of Au in the reaction mixtures. Even if a long time reaction (24 h) was carried out or a large amount of the catalyst (0.1 g) was added, a negligible gold leaching amount is detected after reactions. In a separated test, the oxidation mixture is hot filtered to collect the liquid phase after 2 h stirring under atmospheric pressure. The conversion of benzyl alcohol is 47%. Insignificant change for the conversion of benzyl alcohol after a further 2 h reaction is observed with the same conditions as the initial reaction except in the absence of the solid catalyst (<3%, less than the experimental error). These results clearly suggest that gold leaching could be approximately excluded in the present oxidation reactions. Therefore, the reactions approximately undergo heterogeneous conditions,[40] where the reactant selectively adsorbs on active centers and then converts to the product.

For recycling study, aerobic oxidation of benzyl alcohol was performed maintaining the same atmospheric reaction conditions except using the recovered catalyst. The time plots for the catalytic conversion of benzyl alcohol and yield of benzoic acid over the recovered Au(SH)−C catalyst are similar to those over the fresh one (SI Figure S10). We also tested the initial reaction rate (within 0.5 h) and conversion of benzyl alcohol to benzoic acid at 12 h in successive runs and compiled in Figure 11. It can be clearly found that obvious changes are undetected for catalytic performance after five runs. The reaction mother liquors after hot separation with the catalyst in each run were collected and mixed. The gold content, in the final mixture, is below the detected line by the ICP−AES analysis, implying the negligible metal leaching during the repeated reactions. These results indicate that the gold-containing mesoporous carbon catalyst is stable and can be reused.
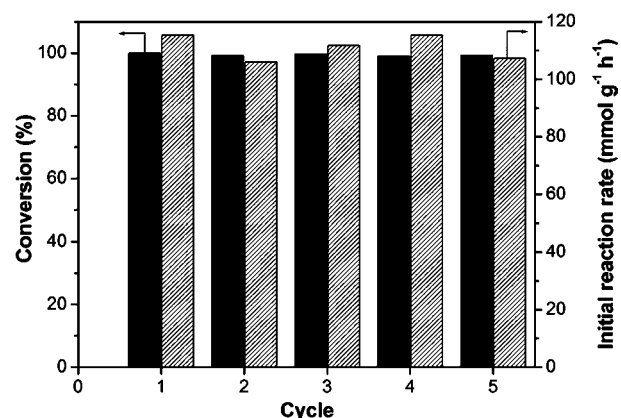

Figure 11. Reusability in terms of conversion of benzyl alcohol and initial reaction rate for the Au(SH)−C catalyst in the selective oxidation of benzyl alcohol at 60 °C under atmospheric pressure.

The XRD patterns, TEM images, and N_2 sorption isotherms clearly show that the reused catalysts retain the ordered mesostructure, high surface area, and uniform mesopores (SI Figures S11, S12, and S13 and Table 1). Obviously, gold nanoparticles are aggregation-free after use. Both the TEM images and WAXRD patterns reveal the particle size of ~9.5 nm, almost the same as the fresh catalyst. The Au(SH)−C−R6 catalyst, after five catalytic runs, shows a gold content of 5.9 wt %, further confirming it is free of metal leaching.

4. DISCUSSION

The synthesis for ordered mesoporous carbon-supported gold nanoparticles involves the one-step coordination-assisted self-assembly approach.

A gold−thiol coordination occurs between Au species and the thiol group in MPTMS in the initial solution, as evidenced by the EXAFS and UV−vis absorption analysis. The coordination can stabilize gold species.[11] Simultaneously, the silane coupling agent containing reactive thiol groups can react with both preformed phenolic resins and TEOS.[41] In this case, the interactions among gold, silane, and resins are strengthened in solution. Triblock copolymer assembly at the interface is originated by the hydrogen-bonding interaction between hydrophilic EO segments and hydroxyl groups of resins and silicates and then induced by solvent evaporation.

The subsequent thermopolymerization step at 100 °C involves further solidification of the integral organic−inorganic frameworks.[26] The so-derived as-made films are flaxen and transparent without obvious macrophase separation. Au in the low chemical state and strong coordination with −SH are very stable. The mobility and reactive ability may therefore be inhibited. The thiol group coordination with gold ions possibly locates either inside the carbonaceous−silicate walls or on the pore surface. By comparison, the lack of coordination of gold ions with thiol moieties is easily reduced to metallic nanoparticles at this stage possibly by unreacted formaldehyde in the phenolic resin.

During heating treatment, the triblock copolymer decom-poses to CO, CH_4, etc. The mesopores are open. Phenolic resins carbonize, and a large amount of small molecules are released. Carbon and silicate form an integrated framework with the ordered mesostructure. The relatively "rigid" inter-penetrated framework is thereafter fixed.[37] Gold species can decompose or reduce to the metallic state. The neighbored

gold species gather together and grow once the thiol groups are released. The growth of gold nanoparticles inside the mesopore channels is feasible with the possibility of penetration into pore walls. However, the particle growth is confined by the rigid silica−carbon framework, and the crystal growth energy in the solidified pore walls is high. As a result, the particles homogenously disperse in the matrix and are confined by the pore walls adjacent to six cylindrical pores. The growth is ended with the particle size about 9.0 nm. Gold seems to "get stuck". The simultaneous formation of gold nanoparticles and a relatively rigid silica−carbon framework favors the intercalation of Au in the pore walls. Unobvious distortion of ordered porosity occurs after gold deposition, although the gold diameter is apparently larger than either the pore size or wall thickness. At the same time, carbon species may deposit over the metallic gold catalysts, in particular at the corner of the interface between the gold and carbonaceous pore wall.[42] These carbon species which can be regarded as part of the carbonaceous pore walls play a further immobilization role in gold nanoparticles. Aggregation of nanoparticles outside nanopores is inhibited. The avoidance of postreduction is interesting because treatment at higher temperatures always generates bigger gold nanoparticles.[43] On contrast, lack of thiol group coordination of gold species will grow to large nanoparticles above 100 nm, move outside pores, and separate with carbon-ordered mesostructure at an elevated temperature, due to the improved immobility of metallic nanoparticles in a relatively "soft" framework.

Therefore, a preformed rigid framework should be favorable for inhibiting growth of small metallic gold clusters during reduction. A preliminary experiment shows that 5.0 nm gold nanoparticles can be confined in the mesoporous carbonaceous framework with an additional low-temperature thermopolymerization at 150 °C, as evidenced by the TEM image and XRD pattern Figure S14, (Supporting Information).

The present catalyst is totally different from the traditional metal catalyst supported by porous carriers. The sintering of gold nanoparticles on the surface of ordered nanopores cannot be avoided due to both the weak interaction between surface and metal and the open nanopores. Metal easily migrates outside the pores to form large particles.[44] The presence of carbon and silica can modify the gold surface energy, and this may result in the expression of "active" surfaces.[45] The space-related growth may also lead to the development of specific facets.[45a] Therefore, the "active" {111} surface is highly exposed.

After removal of the silica component (Au(SH)−C), the carbon wall can support the mesostructure and remain unchanged, only with the generation of plenty of secondary mesopores inside pore walls which are originated from the silica nanoparticles in the interpenetrated framework. The silane coupling agent including the thiol group and silica can be completely eliminated, which would show a negligible effect on the catalytic result of Au-containing mesoporous carbon catalysts. The gold nanoparticles are stable in basic solution. Dissolving and etching can be avoided in this step. The particles are reserved, occupying both pore space and wall, and are exposed. Special corners and edge sites of gold surface atoms may be generated by the secondary pores that are expected by the surprising activity.[45a,46] Besides primary pores, bulky organic molecules can easily enter the secondary mesopores of carbon with the relatively hydrophobic surface.[47] Accordingly, gold nanoparticles are highly accessible. This kind

of carbon support differs from the most reported mesoporous carbon, for example, CMK-3 or FDU-15, whose surface areas are mainly contributed by micropores.[23a,48] Diffusion limitation is much more serious in these cases.[47]

The benzyl alcohol molecules can be enriched inside both primary and secondary mesopores and, therefore, are accessible to gold nanoparticles with highly exposed active surface atoms and special corner or edges. The intermediate alkoxides are first formed and then converted to aldehyde and water by selective C−H bond (α to the oxygen) activation.[49] The Au−H covered catalyst surface might be reactivated by O_2 and OOH. The formation of a strong oxidization agent may facilitate the further oxidation of aldehyde to acid. Simultaneously, the presence of water can reduce the barrier of O_2 hydrogenation.[50] Although benzyl benzoate is also produced, it can be readsorbed on gold nanoparticles and hydrolyze in the presence of aqueous base solution to generate benzoic acid. As a result, benzoic acid is the exclusive oxidation product. Gold nanoparticles, which are confined by the carbon walls, are highly stable. Due to the strong adsorption of benzyl alcohol from water in the mesopores of carbon with the relatively hydrophobic surface, the transportation of soluble thiocyanate is inhibited. As a result, the attack to gold nanoparticles by poison molecules is inhibited. The catalyst exhibits an interestingly poisoning-resistance behavior.

5. CONCLUSION

The one-step construction of the sintering-stable gold-containing mesoporous carbonaceous catalysts is studied on the basis of the coordination-assisted triblock copolymer-templating approach. The silane coupling agent containing the thiol group is essential for the aggregation-free active gold nanoparticles in the carbonaceous matrix, which can coordinate with gold species by the thiol group to obtain monodispersed gold species; react with phenolic resins by silanol groups to form a relatively "rigid" composite framework; and generate secondary pores inside carbon pore walls to provide high surface areas. The silane coupling agent can be completely eliminated with negligible effect on the catalytic performance of Au-containing mesoporous carbon catalysts. During heating treatment, metallic gold is in situ reduced, accompanied with the opening of mesopores and rigidifying of framework. This process facilitates the immobilization and stabilization of monodispersed gold nanoparticles in the carbonaceous framework. Aggregation of nanoparticles is inhibited even with a high carbonization temperature of 600 °C. Once the inorganic component of silica is removed, mesoporous pure carbon-based catalysts can be obtained with maintenance of monodispersed gold nanoparticles (∼9.0 nm), high specific surface area (∼1800 m^2/g), large pore volume (1.19 cm^3/g), and uniform primary pore size distribution (4.0 nm) with plenty of secondary mesopores (<2.0 nm) inside carbon pore walls. The mesoporous carbon-based gold catalyst exhibits an almost complete conversion of benzyl alcohol to benzoic acid within 60 min at 90 °C and 1 MPa, or 12 h at 60 °C and atmospheric pressure. Negligible activity loss, metal leaching, and meso-structure destruction are observed for the reused catalyst. The catalyst is highly poisoning-resistant. Even with a molar ratio for thiocyanate:Au of 33, about 37% activity can be retained. The high activity and stability can be assigned to aggregation-free metallic gold nanoparticles, highly exposed surface atoms by bimodal pores, confinement of nanoparticles by stable carbon mesostructure, and large carbon mesopores with the relatively

hydrophobic surface facilitating the selective adsorption of substrate in water and mass transfer.

■ ASSOCIATED CONTENT

⑤ Supporting Information

Preparation of low-polymerized phenolic resins; Oxidation of benzyl alcohol in water using Au based or bimetallic Au−Pd based supported catalysts; FT-IR spectra and *t*-plots for as-made gold-containing mesoporous catalysts, the catalyst calcined at 600 °C (Au(SH)−SC), and after dissolution of silica (Au(SH)−C); XRD patterns, N₂ sorption isotherms, pore-size distribution curves, and TEM images for the thiol-free sample Au(0)−SC, gold-free sample (SH)−C, supported 5.0 nm gold catalyst, fresh Au(SH)−C catalyst, and the catalysts after the first and third runs (Au(SH)−C−R2 and Au(SH)−C−R4); UV−vis spectra for monoconstituent and biconstituent synthesis solutions in ethanol; and time conversion plots over the reused catalyst Au(SH)−C−R2; and TEM image and WAXRD pattern for the supported 5.0 nm gold catalyst. This material is available free of charge via the Internet at http://pubs.acs.org.

■ AUTHOR INFORMATION

Corresponding Author
ywan@shnu.edu.cn
Notes
The authors declare no competing financial interest.

■ ACKNOWLEDGMENTS

■ REFERENCES

(1) (a) Corma, A.; Leyva-Pérez, A.; Sabater, M. J. *Chem. Rev.* **2011**, *111*, 1657. (b) Corma, A.; Garcia, H. *Chem. Soc. Rev.* **2008**, *37*, 2096. (c) Hashmi, A. S. K.; Hutchings, G. J. *Angew. Chem., Int. Ed.* **2006**, *45*, 7896. (d) Chen, M.; Goodman, D. W. *Acc. Chem. Res.* **2006**, *39*, 739.

(2) Carrettin, S.; Concepción, P.; Corma, A.; López Nieto, J. M.; Puntes, V. F. *Angew. Chem., Int. Ed.* **2004**, *43*, 2538.

(3) Wang, X.; Caruso, R. A. *J. Mater. Chem.* **2011**, *21*, 20.

(4) Fang, W.; Chen, J.; Zhang, Q.; Deng, W.; Wang, Y. *Chem.—Eur. J.* **2011**, *17*, 1247.

(5) Su, F. Z.; Liu, Y. M.; Wang, L. C.; Cao, Y.; He, H. Y.; Fan, K. N. *Angew. Chem.* **2008**, *120*, 340.

(6) Tsunoyama, H.; Sakurai, H.; Negishi, Y.; Tsukuda, T. *J. Am. Chem. Soc.* **2005**, *127*, 9374.

(7) Han, J.; Liu, Y.; Guo, R. *Adv. Funct. Mater.* **2009**, *19*, 1112.

(8) Bore, M. T.; Pham, H. N.; Switzer, E. E.; Ward, T. L.; Fukuoka, A.; Datye, A. K. *J. Phys. Chem. B* **2005**, *109*, 2873.

(9) (a) Narayanan, R.; El-Sayed, M. A. *J. Am. Chem. Soc.* **2003**, *125*, 8340. (b) Chen, C.; Nan, C.; Wang, D.; Su, Q.; Duan, H.; Liu, X.; Zhang, L.; Chu, D.; Song, W.; Peng, Q.; Li, Y. *Angew. Chem., Int. Ed.* **2011**, *50*, 3725. (c) Li, Y.; El-Sayed, M. A. *J. Phys. Chem. B* **2001**, *105*, 8938.

(10) (a) Sun, J.; Ma, D.; Zhang, H.; Liu, X.; Han, X.; Bao, X.; Weinberg, G.; Pfänder, N.; Su, D. *J. Am. Chem. Soc.* **2006**, *128*, 15756. (b) Friedrich, H.; Sietsma, J. R. A.; de Jongh, P. E.; Verkleij, A. J.; de Jong, K. P. *J. Am. Chem. Soc.* **2007**, *129*, 10249. (c) Cargnello, M.; Gentilini, C.; Montini, T.; Fonda, E.; Mehraeen, S.; Chi, M.; Herrera-Collado, M.; Browning, N. D.; Polizzi, S.; Pasquato, L.; Fornasiero, P. *Chem. Mater.* **2010**, *22*, 4335. (d) Budroni, G.; Corma, A. *Angew. Chem., Int. Ed.* **2006**, *45*, 3328. (e) Budroni, G.; Corma, A.; García, H.; Primo, A. *J. Catal.* **2007**, *251*, 345. (f) Laursen, A. B.; Højholt, K. T.; Lundegaard, L. F.; Simonsen, S. B.; Helveg, S.; Schüth, F.; Paul, M.; Grunwaldt, J.-D.; Kegnæs, S.; Christensen, C. H.; Egeblad, K. *Angew. Chem., Int. Ed.* **2010**, *49*, 3504.

(11) (a) Zhu, K.; Hu, J.; Richards, R. *Catal. Lett.* **2005**, *100*, 195. (b) Besson, E.; Mehdi, A.; Reye, C.; Corriu, R. J. P. *J. Mater. Chem.* **2009**, *19*, 4746. (c) Chen, L.; Hu, J.; Richards, R. *J. Am. Chem. Soc.* **2009**, *131*, 914. (d) Wu, P.; Bai, P.; Lei, Z.; Loh, K. P.; Zhao, X. S. *Microporous Mesoporous Mater.* **2011**, *141*, 222. (e) Zhu, F.-X.; Wang, W.; Li, H.-X. *J. Am. Chem. Soc.* **2011**, *133*, 11632.

(12) (a) Wu, S.-H.; Tseng, C.-T.; Lin, Y.-S.; Lin, C.-H.; Hung, Y.; Mou, C.-Y. *J. Mater. Chem.* **2011**, *21*, 789. (b) Botella, P.; Corma, A.; Navarro, M. T. *Chem. Mater.* **2007**, *19*, 1979. (c) Yeung, C. M. Y.; Yu, K. M. K.; Fu, Q. J.; Thompsett, D.; Petch, M. I.; Tsang, S. C. *J. Am. Chem. Soc.* **2005**, *127*, 18010. (d) Joo, S. H.; Park, J. Y.; Tsung, C.-K.; Yamada, Y.; Yang, P.; Somorjai, G. A. *Nat. Mater.* **2009**, *8*, 126. (e) Huang, X.; Guo, C.; Zuo, J.; Zheng, N.; Stucky, G. D. *Small* **2009**, *5*, 361.

(13) Arnal, P. M.; Comotti, M.; Schüth, F. *Angew. Chem., Int. Ed.* **2006**, *45*, 8224.

(14) Wan, Y.; Wang, H.; Zhao, Q.; Klingstedt, M.; Terasaki, O.; Zhao, D. *J. Am. Chem. Soc.* **2009**, *131*, 4541.

(15) (a) Goguet, A.; Hardacre, C.; Harvey, I.; Narasimharao, K.; Saih, Y.; Sa, J. *J. Am. Chem. Soc.* **2009**, *131*, 6973. (b) Sá, J.; Goguet, A.; Taylor, S. F. R.; Tiruvalam, R.; Kiely, C. J.; Nachtegaal, M.; Hutchings, G. J.; Hardacre, C. *Angew. Chem., Int. Ed.* **2011**, *50*, 8912. (c) Dimitratos, N.; Lopez-Sanchez, J. A.; Morgan, D.; Carley, A.; Prati, L.; Hutchings, G. J. *Catal. Today* **2007**, *122*, 317. (d) Simakova, O. A.; Leino, A.-R.; Campo, B.; Mäki-Arvela, P.; Kordás, K.; Mikkola, J.-P.; Murzin, D. Y. *Catal. Today* **2010**, *150*, 32. (e) Galeano, C.; Güttel, R.; Paul, M.; Arnal, P.; Lu, A.-H.; Schüth, F. *Chem.—Eur. J.* **2011**, *17*, 8434.

(16) Prati, L.; Rossi, M. *J. Catal.* **1998**, *176*, 552.

(17) Datta, K. K. R.; Reddy, B. V. S.; Ariga, K.; Vinu, A. *Angew. Chem., Int. Ed.* **2010**, *49*, 5961.

(18) Kerdi, F.; Caps, V.; Tuel, A. *Microporous Mesoporous Mater.* **2011**, *140*, 89.

(19) (a) Dhakshinamoorthy, A.; Alvaro, M.; Garcia, H. *Chem.—Eur. J.* **2011**, *17*, 6256. (b) Nishimura, T.; Kakiuchi, N.; Inoue, M.; Uemura, S. *Chem. Commun.* **2000**, 1245.

(20) Della Pina, C.; Falletta, E.; Rossi, M.; Sacco, A. *J. Catal.* **2009**, *263*, 92.

(21) (a) Haider, P.; Urakawa, A.; Schmidt, E.; Baiker, A. *J. Mol. Catal. A: Chem.* **2009**, *305*, 161. (b) Bayram, E.; Lu, J.; Aydin, C.; Uzun, A.; Browning, N. D.; Gates, B. C.; Finke, R. G. *ACS Catal.* **2012**, *2*, 1947.

(22) Liu, R.; Shi, Y.; Wan, Y.; Meng, Y.; Zhang, F.; Gu, D.; Chen, Z.; Tu, B.; Zhao, D. *J. Am. Chem. Soc.* **2006**, *128*, 11652.

(23) (a) Meng, Y.; Gu, D.; Zhang, F.; Shi, Y.; Yang, H.; Li, Z.; Yu, C.; Tu, B.; Zhao, D. *Angew. Chem., Int. Ed.* **2005**, *44*, 7053. (b) Zhuang, X.; Zhao, Q.; Wan, Y. *J. Mater. Chem.* **2010**, *20*, 4715.

(24) Wilson, K.; Lee, A. F.; Macquarrie, D. J.; Clark, J. H. *Appl. Catal., A* **2002**, *228*, 127.

(25) (a) Thommes, M.; Smarsly, B.; Groenewolt, M.; Ravikovitch, P. I.; Neimark, A. V. *Langmuir* **2006**, *22*, 756. (b) Kleitz, F.; Czuryszkiewicz, T.; Solovyov, L. A.; Lindén, M. *Chem. Mater.* **2006**, *18*, 5070. (c) Groen, J. C.; Peffer, L. A. A.; Pérez-Ramírez, J. *Microporous Mesoporous Mater.* **2003**, *60*, 1.

(26) Meng, Y.; Gu, D.; Zhang, F.; Shi, Y.; Cheng, L.; Feng, D.; Wu, Z.; Chen, Z.; Wan, Y.; Stein, A.; Zhao, D. *Chem. Mater.* **2006**, *18*, 4447.

(27) Süzer, e. *Appl. Spectrosc.* **2000**, *54*, 1716.

(28) (a) Lu, A.-H.; Nitz, J.-J.; Comotti, M.; Weidenthaler, C.; Schlichte, K.; Lehmann, C. W.; Terasaki, O.; Schüth, F. *J. Am. Chem. Soc.* **2010**, *132*, 14152. (b) Wang, W.; Wang, H.-y.; Wei, W.; Xiao, Z.-G.; Wan, Y. *Chem.—Eur. J.* **2011**, *17*, 13461.

(29) Tragoonwichian, S.; O'Rear, E. A.; Yanumet, N. *Colloids Surf., A* **2009**, *349*, 170.

(30) Woehrle, G. H.; Warner, M. G.; Hutchison, J. E. *J. Phys. Chem. B* **2002**, *106*, 9979.

(31) (a) Watkins, J. W.; Elder, R. C.; Greene, B.; Darnall, D. W. *Inorg. Chem.* **1987**, *26*, 1147. (b) Veith, G. M.; Lupini, A. R.; Rashkeev, S.; Pennycook, S. J.; Mullins, D. R.; Schwartz, V.; Bridges, C. A.; Dudney, N. J. *J. Catal.* **2009**, *262*, 92.

(32) (a) Crespo, P.; Litrán, R.; Rojas, T. C.; Multigner, M.; de la Fuente, J. M.; Sánchez-López, J. C.; García, M. A.; Hernando, A.; Penadés, S.; Fernández, A. *Phys. Rev. Lett.* **2004**, *93*, 087204. (b) Alloway, D. M.; Hofmann, M.; Smith, D. L.; Gruhn, N. E.; Graham, A. L.; Colorado, R.; Wysocki, V. H.; Lee, T. R.; Lee, P. A.; Armstrong, N. R. *J. Phys. Chem. B* **2003**, *107*, 11690.

(33) Wang, Z.; Tan, B.; Hussain, I.; Schaeffer, N.; Wyatt, M. F.; Brust, M.; Cooper, A. I. *Langmuir* **2007**, *23*, 885.

(34) Huang, T.; Murray, R. W. *J. Phys. Chem. B* **2003**, *107*, 7434.

(35) (a) Fierro-Gonzalez, J. C.; Gates, B. C. *J. Phys. Chem. B* **2004**, *108*, 16999. (b) Yao, T.; Sun, Z.; Li, Y.; Pan, Z.; Wei, H.; Xie, Y.; Nomura, M.; Niwa, Y.; Yan, W.; Wu, Z.; Jiang, Y.; Liu, Q.; Wei, S. *J. Am. Chem. Soc.* **2010**, *132*, 7696.

(36) (a) Shimizu, T.; Teranishi, T.; Hasegawa, S.; Miyake, M. *J. Phys. Chem. B* **2003**, *107*, 2719. (b) Navalon, S.; de Miguel, M.; Martin, R.; Alvaro, M.; Garcia, H. *J. Am. Chem. Soc.* **2011**, *133*, 2218.

(37) Wang, W.; Zhuang, X.; Zhao, Q.; Wan, Y. *J. Mater. Chem.* **2012**, *22*, 15874.

(38) (a) Noyori, R.; Aoki, M.; Sato, K. *Chem. Commun.* **2003**, 1977. (b) Tsukinoki, T.; Tsuzuki, H. *Green Chem.* **2001**, *3*, 37. (c) Wan, Y.; Zhang, D.; Zhai, Y.; Feng, C.; Chen, J.; Li, H. *Chem. Asian J.* **2007**, *2*, 875.

(39) (a) Dimitratos, N.; Lopez-Sanchez, J. A.; Hutchings, G. J. *Chem. Sci* **2012**, *3*, 20. (b) Liu, Y.; Tsunoyama, H.; Akita, T.; Tsukuda, T. *J. Phys. Chem. C* **2009**, *113*, 13457. (c) Liu, Y. M.; Tsunoyama, H.; Akita, T.; Tsukuda, T. *Chem. Lett.* **2010**, *39*, 159. (d) Ma, C. Y.; Dou, B. J.; Li, J. J.; Cheng, J.; Hu, Q.; Hao, Z. P.; Qiao, S. Z. *Appl. Catal., B* **2009**, *92*, 202. (e) Villa, A.; Janjic, N.; Spontoni, P.; Wang, D.; Su, D. S.; Prati, L. *Appl. Catal., A* **2009**, *364*, 221.

(40) Casanova, O.; Iborra, S.; Corma, A. *J. Catal.* **2009**, *265*, 109.

(41) Takeichi, T.; Guo, Y.; Agag, T. *J. Polym. Sci., Part A: Polym. Chem.* **2000**, *38*, 4165.

(42) Ellis, A. V.; Vijayamohanan, K.; Goswami, R.; Chakrapani, N.; Ramanathan, L. S.; Ajayan, P. M.; Ramanath, G. *Nano Lett.* **2003**, *3*, 279.

(43) Zanella, R.; Sandoval, A.; Santiago, P.; Basiuk, V. A.; Saniger, J. M. *J. Phys. Chem. B* **2006**, *110*, 8559.

(44) Ma, Z.; Dai, S. *ACS Catal.* **2011**, *1*, 805.

(45) (a) Schaetz, A.; Zeltner, M.; Stark, W. J. *ACS Catal.* **2012**, *2*, 1267. (b) Ariga, K.; Vinu, A.; Yamauchi, Y.; Ji, Q. M.; Hill, J. P. *Bull. Chem. Soc. Jpn.* **2012**, *85*, 1.

(46) (a) Comotti, M.; Li, W.-C.; Spliethoff, B.; Schüth, F. *J. Am. Chem. Soc.* **2005**, *128*, 917. (b) Lopez, N.; Janssens, T. V. W.; Clausen, B. S.; Xu, Y.; Mavrikakis, M.; Bligaard, T.; Nørskov, J. K. *J. Catal.* **2004**, *223*, 232. (c) Mohr, C.; Hofmeister, H.; Radnik, J.; Claus, P. *J. Am. Chem. Soc.* **2003**, *125*, 1905. (d) Lopez, N.; Nørskov, J. K. *J. Am. Chem. Soc.* **2002**, *124*, 11262.

(47) Zhuang, X.; Wan, Y.; Feng, C.; Shen, Y.; Zhao, D. *Chem. Mater.* **2009**, *21*, 706.

(48) Jun, S.; Joo, S. H.; Ryoo, R.; Kruk, M.; Jaroniec, M.; Liu, Z.; Ohsuna, T.; Terasaki, O. *J. Am. Chem. Soc.* **2000**, *122*, 10712.

(49) (a) Shang, C.; Liu, Z.-P. *J. Am. Chem. Soc.* **2011**, *133*, 9938. (b) Tsunoyama, H.; Ichikuni, N.; Sakurai, H.; Tsukuda, T. *J. Am. Chem. Soc.* **2009**, *131*, 7086. (c) Ketchie, W. C.; Fang, Y.-L.; Wong, M. S.; Murayama, M.; Davis, R. J. *J. Catal.* **2007**, *250*, 94. (d) Yang, X.; Wang, X.; Liang, C.; Su, W.; Wang, C.; Feng, Z.; Li, C.; Qiu, J. *Catal. Commun.* **2008**, *9*, 2278.

(50) Ketchie, W.; Murayama, M.; Davis, R. *Top. Catal.* **2007**, *44*, 307.